**Energy Equipment and Systems**

# A numerical study of the effect of channel spacers on the performance of cross-flow forward osmosis membrane modules

Authors

**Alireza Jalali** [a*]
**Naeem Niknafs** [a]

[a] School of Mechanical Engineering, College of Engineering, University of Tehran, North Kargar Avenue, Tehran,1439957131, Iran

ABSTRACT

*In this paper, we perform two-dimensional simulations of cross-flow forward osmosis (FO) membrane modules in the presence of draw and feed channel spacers. For this purpose, the equations corresponding to the conservation of mass, momentum, and convection-diffusion for the mass fraction of solute are solved using a commercial finite volume flow solver. We consider six configurations of channel spacers being constructed by the symmetric and asymmetric placement of cavity, submerged, and zigzag arrangements. We will study the effect of the spacers' geometrical parameters such as diameter and relative distance in these configurations as well as the solute resistivity of the porous support layer on the performance of the FO membrane modules in terms of water flux, external concentration polarization (ECP) factors, and pressure drop per unit length of the membrane. Our results reveal that increasing the solute resistivity of the porous support layer has an adverse effect on the water flux, whereas the impact on the ECP factors is positive. In addition, it turns out that the submerged configurations, where the spacer filaments are not in direct contact with the membrane surface, produce the highest water flux through the membrane; however, they have an adverse effect on the pressure drop along the membrane surface.*

## 1. Introduction

Exponential population growth and rapid industrialization have severe impacts on the world's freshwater resources. Due to uneven freshwater demand and supply around the world, more than one-third of the world's population is living in water-stressed regions [1]. Therefore, the production of freshwater from other resources has become more crucial in recent years. Seawater desalination and wastewater treatment are among the alternatives to deliver freshwater in the regions with serious water scarcity problems.

Pressure-driven membrane-based separation technologies, such as nanofiltration (NF) and reverse osmosis (RO), are the most widely used techniques to produce high-quality freshwater from seawater and wastewater [2]. These processes require a massive amount of energy to provide the net external pressure required to overcome the difference in osmotic pressure. On the other hand, forward osmosis (FO), a new osmotic-driven membrane-based separation technique, has received significant

* Corresponding author: Alireza Jalali
School of Mechanical Engineering, College of Engineering, University of Tehran, North Kargar Avenue, Tehran,1439957131, Iran
Email: arjalali@ut.ac.ir

attention in the past decade due to its lower energy requirements. In this process, a concentrated draw solution with a high osmotic pressure draws water molecules through a semi-permeable membrane from a feed solution. The diluted draw solution is then recovered to maintain the higher osmotic pressure on the draw side, and produce high-quality pure water. Since the driving force is only the difference in the osmotic pressure of the two solutions, there is no need to consume extra energy sources.

In the RO process, the high pressure applied on the concentrated side of the membrane causes the rejected salt to accumulate in the vicinity of the membrane surface. This phenomenon, which leads to a difference in the concentration of salt between the membrane surface and the bulk solution, is known as the external concentration polarization (ECP). In addition, the dilute solution traveling through the porous support layer causes a minimal difference in the salt concentration between the two sides of the support layer, referred to as the internal concentration polarization (ICP). In the FO process; however, water penetrates from a low concentrated solution into a highly concentrated solution. As a result, the dilutive and concentrative ECP (i.e., DECP and CECP) occur on the two sides of the membrane, followed by a strong ICP in the porous support layer. In FO, the concentration polarization may considerably reduce mass transfer by lowering the effective driving force for water permeation. A standard practice in the production of spiral wound membranes (SWMs) uses channel spacers to keep the membrane leaves apart, enhancing mass transfer through the membrane.

To study the effect of different geometrical parameters of the spacers on mass transfer, it is possible to take advantage of computational fluid dynamics (CFD). With the recent advancements in computational power and thus, the capability of performing simulations on high-resolution meshes, very accurate predictions of transport phenomena in membrane processes can be obtained [3]. Using CFD, the field properties such as flow velocity and salt concentration can be computed at arbitrary points of a computational domain. Additionally, CFD enables us to investigate the effect of different thermo-physical properties and geometrical

arrangements on membranes' performance without the need to create the cases in reality [4,5].

In several studies, CFD has been employed to study transport phenomena in FO membranes. Park *et al.* [6] developed a finite element method (FEM). The model successfully determined a constant membrane structure parameter that is solely dependent on the membrane's intrinsic parameters such as thickness and the porosity and tortuosity of the support layer, as opposed to experimental studies that produced various values for the same membrane properties. Sagiv and Semiat [7] used a two-dimensional FEM model to solve the mass and momentum transport equations for FO desalination with NaCl solutions. They discovered that the major reduction in water permeation through the membrane comes from the CP layer on the draw side; therefore, draw solution concentration must be optimized to obtain an effective driving force. With the inspiration received from the modeling of pressure-driven RO systems and analytic flux modeling, Gruber *et al.* developed a powerful CFD model to simulate FO asymmetric membranes without spacers [8]. Their model revealed that, unlike common assumptions, the ECP on the porous surface of asymmetric FO membranes is not negligible in realistic conditions. Later, Park and Kim [9] used a two-dimensional CFD model to study the impact of spacers on the concentration polarization in a FO process. They investigated the effect of spacers' configurations in various concentration conditions and introduced an index named CPI to compare the degree of CP between different spacer arrangements. However, they did not address the effect of spacers' diameter and relative distance on FO membrane performance. Their study showed that the boundary layer compression is the most effective mechanism to reduce CP in FO membranes in contrast to RO systems where boundary layer disruption is effective. Also, Sagiv *et al.* numerically investigated the performance of a FO membrane with a composite channel structure by solving two-dimensional fully coupled fluid flow and mass transfer equations [10]. The composite structure comprised feed and draw channels, as well as the membrane's active and support layers. Their model was capable of considering co-current and counter-current

operations where the active layer of the membrane faces the feed or draw solutions. The results indicated that FO operation in counter-current mode, while the active layer faces the draw solution leads to a slight improvement in water flux and reduced migration of feed and draw solutes. In another study, Gruber *et al.* presented an optimized open-source three-dimensional CFD solver for the steady-state and transient simulation of RO and FO membranes [11]. They demonstrated the capability of their solver for FO by investigating the effect of different flow and geometry parameters on the performance of a lab-scale membrane module. The results suggested that varying the inlet angle, or the number of inlets, have little influence on the total mass transfer. They also showed that the model is capable of evaluating mass transfer for different arrangements of spacers by the analysis of how spacer geometry affects dead volumes with low flow in the module. Quite recently, Kahrizi *et al.* employed two approaches to study a FO process [12]. A mathematical formulation based on mass transfer resistances and bulk concentration differences was used in the first approach. A more sophisticated approach based on the CFD modeling of the membrane in two-dimensions was utilized to provide a more realistic representation of the FO membrane. They evaluated the forward water and reverse salt fluxes using both approaches. Their CFD results revealed that these fluxes are dependent on the ratio of membrane porosity to its tortuosity. Therefore, it is possible to control ICP and reverse salt diffusion by careful tuning of this parameter.

In this paper, we will develop a two-dimensional CFD model of a cross-flow FO system with feed and draw solution channels. The six spacers' arrangements introduced in

Park and Kim's study [9] are used to investigate the effect of spacers' diameter and relative distance alongside the solute resistivity of the porous support layer on FO membrane performance. Specifically, the water permeation flux, the pressure drop along the membrane, the dilutive ECP in the draw channel, and the concentrative ECP in the feed channel are the parameters by which we will compare different modules' performances with each other.

## 2. Numerical Simulation

In this study, ANSYS Fluent 19.4 was employed to perform a finite-volume-based numerical simulation of the FO process in a composite membrane system with channel spacers. In this section, we will describe the geometry of the problem considered, including the channels and spacers' configurations. Also, we will explain the equations governing the physics of the problem, along with the appropriate boundary conditions. Finally, we will introduce the parameters of the membrane by which we will evaluate the performance of the process.

### 2.1. Simulation domain

The geometry of the domain, being simulated in this paper (Fig. 1), is comprised of feed and draw channels with different arrangements of spacers.

The membrane is operated in the counter-current mode, i.e., the flow direction in the feed and draw channels with an equal height of $h$ is opposite. The membrane thickness, which includes a porous support layer and an active layer, is not resolved in this study. Nevertheless, the effect of the porous layer is considered by an appropriate boundary condition, as will be discussed later.
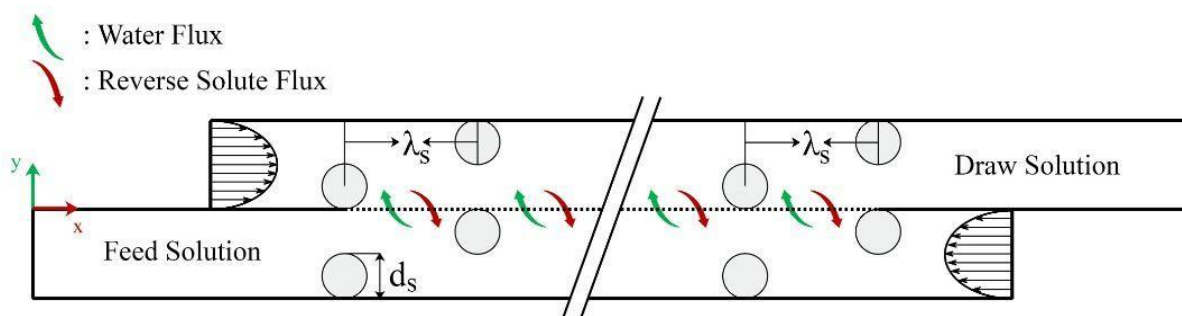


**Fig. 1.** Schematic representation of the geometry of the FO membrane with channel spacers

In two-dimensional simulations of RO membranes, three spacer configurations in the feed channel are used: cavity, submerged, and zigzag [13,14]. However, six spacers' configurations introduced by Park and Kim [9] are investigated due to the importance of ECP in both channels of FO membranes. These configurations are made by symmetric and asymmetric placements of the cavity, submerged, and zigzag configurations with respect to the membrane surface, as shown in Fig. 2. These configurations are named by two letters: the first letter determines symmetric or asymmetric placement (S and A), and the second letter refers to configuration type (C, S, and Z). In the cases of the cavity and zigzag configurations, the sharp angle created near the contact points with the membrane or channel walls results in highly skewed cells in the mesh, which hamper the convergence of the numerical solution. Therefore, the diameter of the spacer filaments, $d_s$, is extended by 1% to make a minuscule overlap with those surfaces. It should be noted that a lower amount of extension, unnecessarily escalates the computational cost and difficulty by producing a high number of minute and sharp-angled cells. This strategy, which has successfully been applied for the simulation of RO membranes [15], prevents the formation of highly skewed cells in the mesh with no considerable error in the results. Each channel includes ten spacers with a relative distance of $\lambda_s$ and equal diameters. In each case, the height and length of each channel are set to $h = 2d_s$ and $L = 9\lambda_s$ (for AC and AS configurations $L = 9.5\lambda_s$), respectively. An entrance length of 5 mm is provided for each channel to ensure that the inflow is not obstructed by the spacer filaments. Also, the length of the channels is extended by $20d_s$

from the end to prevent the influence of outlet boundary condition on the flow.

## 2.2. Governing equations and boundary conditions

The flow in the membrane is assumed to be steady, laminar, Newtonian, and isothermal. The governing equations that describe the transport phenomena in the membrane channels include the conservation of mass, momentum, and convection-diffusion equation for the mass fraction of solute in two-dimensions:

$$\nabla \cdot (\rho \vec{V}) = 0 \tag{1}$$

$$\nabla \cdot (\rho \vec{V} V_i) = -\nabla P + \nabla \cdot [\mu(\nabla \vec{V} + \nabla \vec{V}^T)] \tag{2}$$

$$\nabla \cdot (\rho \vec{V} m_A) - \nabla \cdot [\rho D_{AB}(\nabla m_A)] = 0 \tag{3}$$

where $\rho$ is the fluid density, $\vec{V} = (u, v)$ is the velocity vector, $P$ is the fluid pressure, $\mu$ is the fluid dynamic viscosity, $m_A$ is the solute mass fraction, and $D_{AB}$ is the solute mass diffusivity. For lab-scale cross-flow membrane chambers, where initial volumes of draw and feed solutions getting recirculated, the modeling should be carried out in transient mode, since the water permeation from the feed side to the draw channel and the reverse solute flux from the draw side to the feed channel cause the draw and feed solutions get diluted and concentrated over time, respectively. However, our modeling was performed in the steady-state condition to represent the flow in actual cross-flow FO membrane elements, such as Spiral-Wound Modules (SWMs), where a constant flow of draw and feed solutions with a fixed concentration is available at the module's inlets.
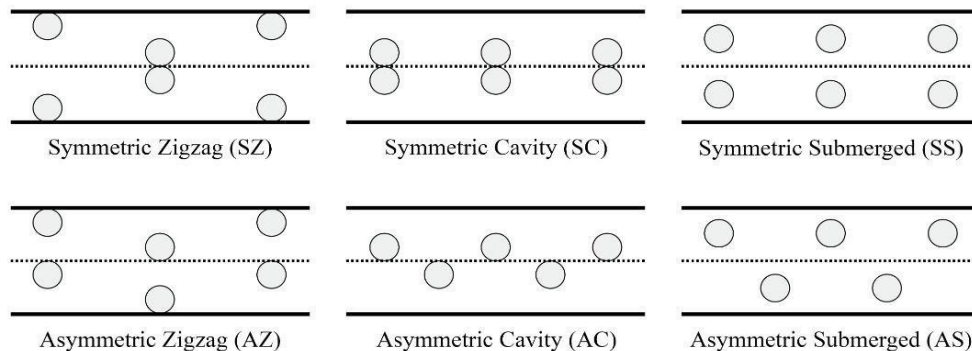


**Fig. 2.** The six configurations of channel spacers for FO membrane
.

The fluid density, viscosity, and solute mass diffusivity are assumed to be dependent on the mass fraction of solute based on an empirical relation reported by Geraldes *et al.* [16] for a NaCl solution at 25°C:

$$\rho = 997.1 + 694\, m_A \tag{4}$$

$$\mu = 0.89 \times 10^{-3}(1 + 1.63\, m_A) \tag{5}$$

$$D_{AB} = \max\begin{pmatrix} 1.61 \times 10^{-9}(1 - 14\, m_A) \\ , 1.45 \times 10^{-9} \end{pmatrix} \tag{6}$$

At the inlet of each channel, a uniform mass fraction of solute is considered. Also, the fully-developed velocity profile at the inlet of the two channels is given by:

$$u = 6\bar{U}\frac{y}{h}\left(1 \mp \frac{y}{h}\right) \tag{7}$$

where $u$ is the *x*-direction velocity component, $\bar{U}$ is the average velocity in the channel, and $h$ is the height of each channel. Note that due to the counter-current arrangement of the membrane, the negative and positive terms correspond to the upper and lower channels, respectively. At the outlets, a gauge pressure of zero, $P = 0$, is specified, and the gradient of the solute mass fraction is assumed to be zero along the channels (i.e., $\partial m_A/\partial n = 0$). On all non-membrane walls of the domain, the no-slip condition, $\vec{V} = 0$, and a zero normal gradient of solute mass fraction, $\partial m_A/\partial n$, are imposed as boundary conditions.

As noted before, the membrane is modeled as a zero thickness plane, which separates the two channels. Considering that the presence of a porous support layer influences the concentration of solute and thus the osmotic pressure across the membrane, additional information must be incorporated to make the model mimic the real condition of the membrane. For this purpose, a well-accepted analytic model, developed by Leob *et al.* [17], is utilized to describe the effect of the porous support layer on water permeation flux, $\vec{J}_w$:

$$\vec{J}_w = \frac{1}{K}\ln\frac{B + A\pi_{d,m}}{B + |\vec{J}_w| + A\pi_{f,m}}\hat{n}_d \tag{8}$$

where $A$ is the water permeability coefficient, $B$ is the solute permeation coefficient, and $K$ is the solute resistivity of the support layer. The constants $A$, $B$, and $K$ are determined experimentally for a membrane. In addition,

$\pi_{d,m}$ is the membrane osmotic pressure on the draw side, and $\pi_{f,m}$ is the membrane osmotic pressure on the feed side. It is assumed that the osmotic pressure at any point is linearly dependent on the solute mass fraction. An empirical relation for NaCl solution at 25°C suggests that $\pi = 805.1 \times 10^5 m_A$ [16]. Note that Eq. (8) gives the water permeation flux implicitly and thus Ridder's root finding method [18] is applied for each point on the membrane to get $\vec{J}_w$. The water flux is used to set the membrane boundary velocity in the normal direction, $\hat{n}_d$. The no-slip boundary is enforced in the tangential direction.

To provide a boundary condition for the solute mass fraction, we pay our attention to the solute flux through the membrane. The total solute flux, $\vec{J}_s$, is obtained as the sum of the convective and diffusive fluxes as:

$$\vec{J}_s = -\rho_m D_{AB}\frac{\partial m_A}{\partial n_d}\hat{n}_d + \rho_m m_{A,m}\vec{J}_w \tag{9}$$

where subscript $m$ refers to the properties evaluated at the membrane surface. Equation (9) must be satisfied on both sides of the membrane. Assuming a linear relation between the osmotic pressure, $\pi$, and solute concentration, $C$, Gruber et al. [8] argued that

$$\vec{J}_s = -\frac{B}{\phi.A}\vec{J}_w \tag{10}$$

where $\phi$ is the constant of proportionality between the osmotic pressure and solute concentration (i.e., $\pi = \phi.C$). For the NaCl solution considered in this study, $\phi = 805 \times 10^2$ Pa m$^3$ kg$^{-1}$. Having computed the water flux, the boundary condition for the solute mass fraction is readily available by Eq. (9).

### 2.3. Performance Parameters

To evaluate the performance of FO membranes with different spacers' configurations, several parameters are calculated based on the numerical solution. These parameters include the averaged water flux across the membrane, dilutive and concentrative ECP, and pressure drop along the feed channel.

The water flux going through the membrane is obtained by Eq. (8). The averaged flux of water is computed in each

case to assess the capability of the membrane for water permeation.

The averaged mass fraction of solute is computed on the feed and draw sides of the membrane to calculate measures of dilutive and concentrative ECP. These averaged values are denoted by $(\overline{m}_{A,f})_m$ and $(\overline{m}_{A,d})_m$ for the feed and draw sides, respectively. In addition, the averaged values of bulk mass fractions, denoted by $(\overline{m}_{A,f})_b$ and $(\overline{m}_{A,d})_b$, are computed on the horizontal mid-lines of each channel at $y = \pm h/2$. Having computed the averaged mass fractions, DECP and CECP factors can be obtained as:

$$DECP = \frac{(\overline{m}_{A,d})_m}{(\overline{m}_{A,d})_b}, \qquad (11)$$

$$CECP = \frac{(\overline{m}_{A,f})_m}{(\overline{m}_{A,f})_b}$$

To investigate the effect of spacers' geometry on the pressure drop, the averaged pressure on the inlet and outlet of the feed channel can be attained ($\overline{P}_{in}$ and $\overline{P}_{out}$). Since the membrane length varies with the relative distance of spacers, the pressure drop is divided by the membrane length to provide a more rigorous estimate of geometry effect on the pressure drop.

## 3. Results and discussions

The simulation results presented in this section were run on a personal computer with an i5-2450M CPU at 2.5 GHz. In all cases, the convergence process continues until the $L_2$-norm of residuals corresponding to the steady-state continuity, momentum, and species transport equations drops below $10^{-6}$. It was also ensured that the change in the solute mass fraction on the feed side of the membrane is less than $10^{-4}$ when the solution is reached. The results include the verification case performed for the governing equations and boundary conditions, grid convergence study carried out to find the proper mesh size, and the study of the effect of different membrane module parameters on FO module performance. The membrane water permeability and solute permeation coefficients are assumed to be $A = 10^{-12} \, m \, (s.Pa)^{-1}$, and $B = 10^{-7} \, m.s^{-1}$. Also, the averaged velocity

magnitude in both the feed and draw channels is $\overline{U} = 0.1 \, m.s^{-1}$, in all cases.

### 3.1. Verification

To verify the correct implementation of governing equations and boundary conditions discussed in Section 2.2, we consider a two-dimensional FO membrane without spacers, which was thoroughly studied by Gruber *et al.* [8]. The governing equations and boundary conditions in their study are identical to the ones mentioned in this paper.

For this test case, the length and height of the two channels are $L = 14 \, mm$, and $h = 3 \, mm$, respectively. In the model developed by Gruber *et al.* [8], a Cartesian mesh with cells having a size of approximately $0.05 \, mm$ near the channels' walls, and with a height of $5 \, \mu m$ near the membrane surface was used. However, in our model, the same mesh routine implemented for the spacer-filled channels, which will be described in Section 3.2, is utilized. The verification is carried out by considering two sets of simulations; each includes 9 cases. In the first set, the mass fraction of solute at the feed inlet is set to $m_A = 0$ while $m_A$ values at the draw inlet vary from 0.01 to 0.09 at the feed inlet. In the second set, $m_A = 0.09$ is kept constant at the draw inlet while $m_A$ values are changed from 0.01 to 0.09. The solute resistivity of the porous support layer is assumed to be $K = 0.5 \, s.\mu m^{-1}$. Figure 3 compares the water mass flux through the membrane between our study and Gruber *et al.* [8] in each case. As expected, the increase in the osmotic pressure difference across the membrane results in a water flux increase. In addition, the values obtained by our model are in good agreement with Ref. [8], verifying the correct implementation of equations and boundary conditions in our work.

### 3.2. Grid Convergence Study

To find out the proper mesh size for the simulation of FO membranes with different spacers' arrangements, the sensitivity of some outputs to the mesh size was investigated. For this purpose, we considered a membrane with $K = 0.5 \, s.\mu m^{-1}$ and spacers' arrangement of SZ (symmetric zigzag) where $d_s = 0.5 \, mm$, and $\lambda_s = 4.5 \, mm$. The solute mass fraction,

$m_A$, at the inlets of feed and draw channels were set to 0.001 and 0.06, respectively.

The domain was tessellated with unstructured meshes. The regions near the membranes and spacers are also appropriately refined to capture the gradients of flow properties (Fig. 4).

For grid independency study, the meshes are systematically refined so that the length scale is almost reduced by a factor of two in each level of refinement. Table 1 shows the water flux in terms of litre per meter squared per hour (LMH), and also the averaged solute mass fraction on the feed and draw sides of the membrane for three different mesh sizes.
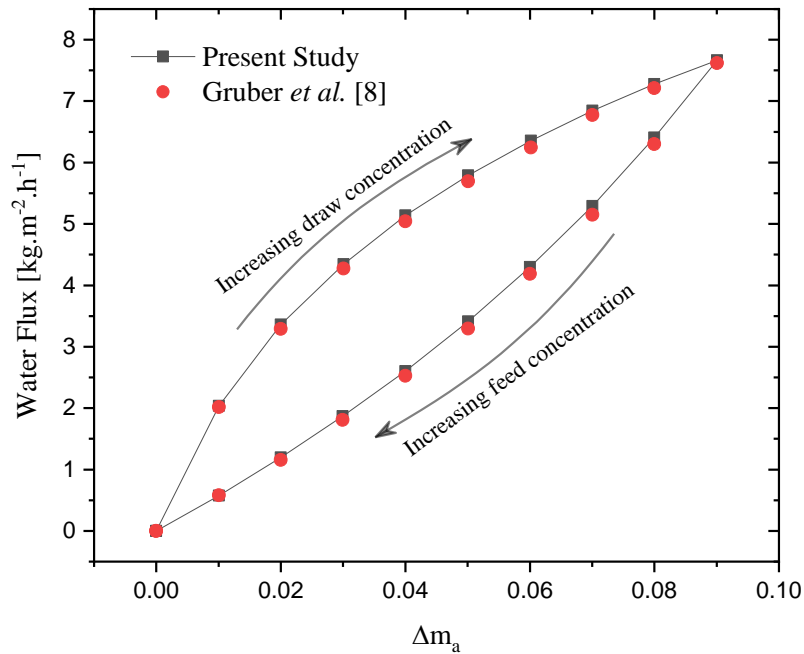


**Fig. 3.** Effect of the solute mass fraction difference on water mass flux (verification of our model results with Ref. [8])
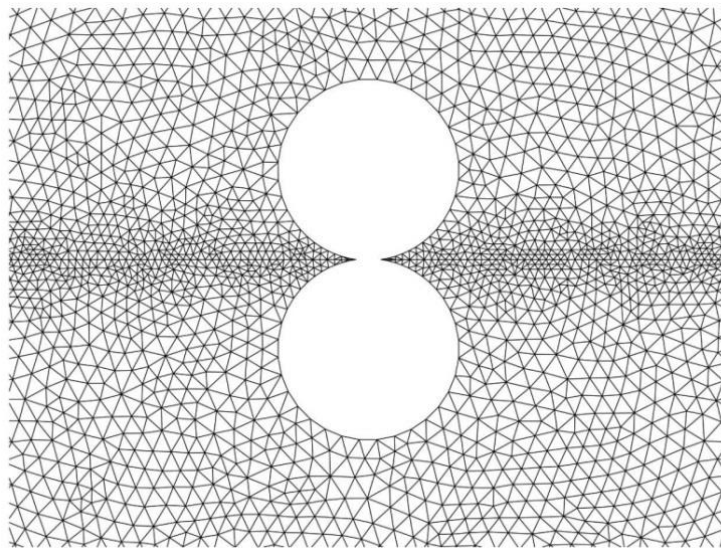


**Fig. 4.** Representation of the mesh used for CFD simulation of FO membranes with channel spacers

**Table 1.** Grid Convergence Index (GCI) of output parameters for a FO membrane with SZ spacers' configurations

| Mesh | No. of Cells | Water flux (LMH) | $\left(\overline{m}_{A,f}\right)_m$ | $\left(\overline{m}_{A,d}\right)_m$ |
|---|---|---|---|---|
| Coarse | 31654 | 6.361053 | 0.001103 | 0.057528 |
| Medium | 119659 | 6.349721 | 0.00111 | 0.057355 |
| Fine | 420144 | 6.327175 | 0.00112 | 0.05701 |
| GCI (%) | | 0.3836 | 1.7779 | 0.6452 |

For theses meshes, the grid convergence indexes (GCIs) for the output parameters have been tabulated. The reported indexes show that the medium mesh with 119,659 cells, where the averaged cell size is 0.02 mm near the membrane with the growth rate of 1.15 and 0.05 mm elsewhere, is fine enough to resolve the flow field properly. So, we decompose the other computational domains with the same mesh size.

### 3.3. Membrane parametric study

In this section, we turn our attention to the effect of some membrane parameters on the performance of FO modules. In particular, we consider solute resistivity of porous support layer ($K$ values) as well as spacers' diameter, and relative distance for different configurations introduced earlier. In all cases, the mass fraction of solute at the inlets of draw and feed channels are 0.06 and 0.001, respectively.

Figure 5 depicts the effect of spacers' diameter and relative distance in AC configuration on the water flux through the membrane at three different $K$ values. As $K$ decreases, the water flux through the

membrane increases. The amount of ICP in the membrane porous support layer declines as $K$ decreases. So the concentration difference between the two sides of the membrane increases, which leads to an increase in water flux. As seen in Fig. 5a where $\lambda_s = 4.5\ mm$, increasing $d_s$ augments the volume of the dead zone in the vicinity of the interface between the spacers and membrane in AC configuration. Consequently, the solute accumulation in the dead zone leads to the reduction of concentration difference across the membrane and thus water flux. The accumulation of solute in the dead zone can also be generalized to the other configurations where the spacers are in contact with the membrane. As seen in Fig. 5b where $d_s = 0.5\ mm$, the variation of the relative distance between spacer filaments does not have a significant effect on the water flux as it changes the concentration difference between the two sides of the membrane only slightly. As the distance increases, the volume of the dead zone per unit length of the membrane surface decreases; thus, the water flux somewhat increases.
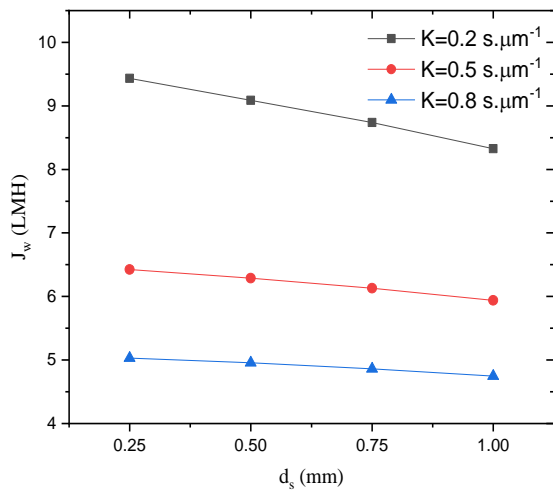


(a) Water flux vs. spacers' diameter for different $K$ values ($\lambda_s = 4.5\ mm$)
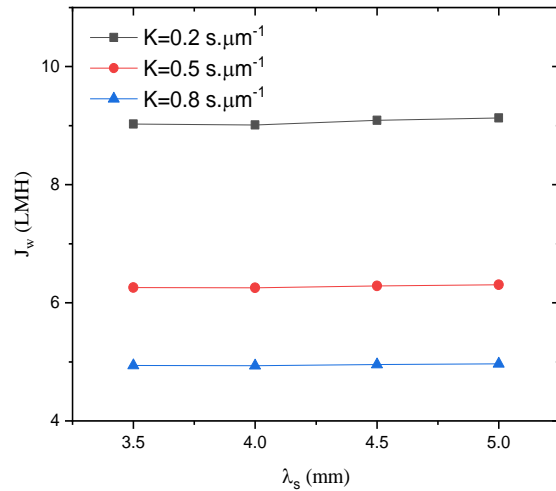
(b) Water flux vs. spacers' relative distance for different $K$ values ($d_s = 0.5\ mm$)

**Fig. 5.** Effect of spacers' geometry on water flux in the AC configuration

Likewise, we can compute the values of the CECP and DECP factors for the AC configuration at three different $K$ values. Figure 6 shows these factors versus the two geometrical parameters. As the distance between the spacers increases, the CECP factor decreases while the DECP factor increases, which can be explained by the reduction of dead zone volume where the solute is trapped. So in a certain length of the membrane, a lower amount of solute is trapped in the interface between the spacers and membrane on the feed side, leading to a decrease in CECP. Also, the spacers on the draw side of the membrane hinder a proper recirculation of water; thus, the draw solution dilutes locally, leading to an increase in the DECP factor. However, with a further decrease in the distance between the spacers,

the high amount of turbulence created by the spacers restricts further increase in CECP and decrease in DECP by augmenting recirculation in the dead zone. As the diameter of the spacers increases, the amount of the dead zone per unit length of the membrane increases, which leads to an increase in CECP and a decrease in the DECP factor. The variation of CECP and DECP is more pronounced in low values of $K$ as the reverse solute flux, $J_s$, increases due to lower ICP and higher concentration difference. So, a higher amount of solute is trapped in the dead zone, leading to an increase in CECP. Also, the value of water flux, $J_w$, increases as $K$ decreases, leading to more dilution of the draw solution in the vicinity of the spacers in the draw channel.
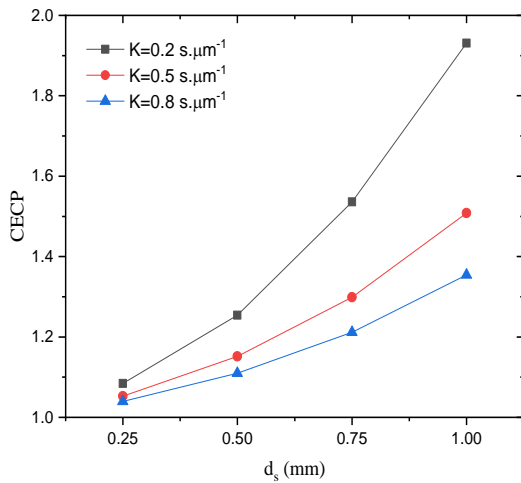


(a) CECP vs. spacers' diameter for different $K$ values ($\lambda_s = 4.5\ mm$)
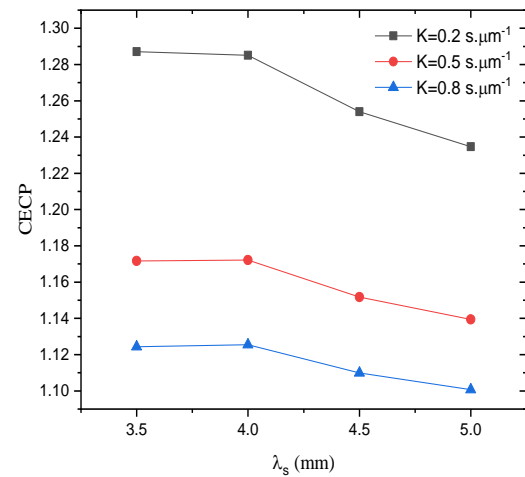
(b) CECP vs. spacers' relative distance for different $K$ values ($d_s = 0.5\ mm$)
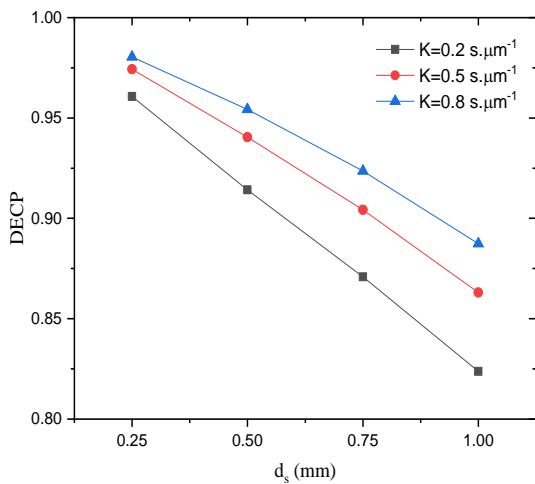
(c) DECP vs. spacers' diameter for different $K$ values ($\lambda_s = 4.5\ mm$)
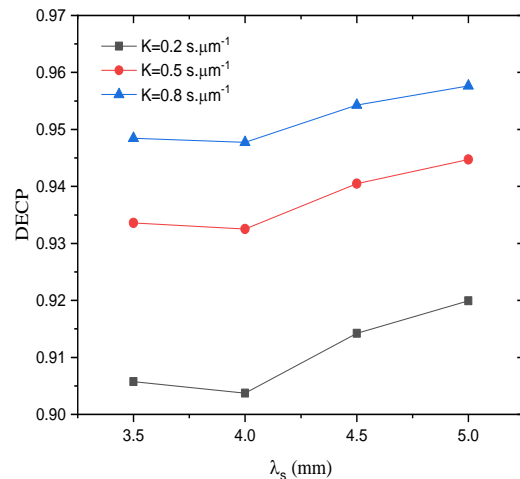
(d) DECP vs. spacers' relative distance for different $K$ values ($d_s = 0.5\ mm$)

**Fig. 6.** Effect of spacers' geometry on external concentration polarization factors in the AC configuration

To investigate the effect of spacers' arrangement on the performance of the membrane, the values of the water flux are compared among the six arrangements at a constant value of $K = 0.5 \, s.\mu m^{-1}$. Figure 7 shows how the water flux changes in terms of spacers' diameter and relative distance for each arrangement. The cavity configurations have the least water flux among the configurations as they have the highest volume of dead zone per unit length of the membrane surface, which notably decreases the effective concentration difference between the two sides of the membrane. The zigzag configurations have higher water fluxes comparing with the cavity configurations. The reason is that in the zigzag configurations, fewer spacers are in contact with the membrane surface, so the volume of the dead zone per unit length of the membrane is smaller. In addition, the turbulence caused by the spacers that are not in contact with the membrane surface augments recirculation in the draw and feed solutions, mitigating the detrimental effect of the dead zone. The submerged configurations have the highest water flux since there is no dead zone available on their membrane surface. As the distance between the spacers increases, less turbulence is created in the channels, which leads to an increase in ECP

on both sides of the membrane and decreases the water flux. As the diameter of the spacers increases, the depth of the channels increases accordingly (the depth of the channels is twice as large as the spacers' diameter). So the velocity gradient in the channels decreases, and subsequently, the shear stress on the membrane layer decreases, which leads to a slight reduction of the water flux. Nevertheless, when the diameter increases to 1mm, the high amount of turbulence created by larger spacers dominates and increases the water flux slightly.

Similarly, the values of the CECP and DECP factors can be computed for each configuration. Figure 8 shows these factors in terms of spacers' geometry. The behaviour of the ECP factors can be explained exactly by the conclusions drawn for the behaviour of the water flux in each configuration.

To study the effect of solute resistivity of the porous support layer on the performance of FO membranes, the water flux can be computed for each configuration (Fig. 9). As seen, all of the configurations follow similar behaviour as ICP is the foremost cause of water flux decline in FO, and the value of $K$ is directly related to the amount of ICP. It should be noted that the effect of tangent spacers in water flux reduction is insignificant compared with the impact of $K$.
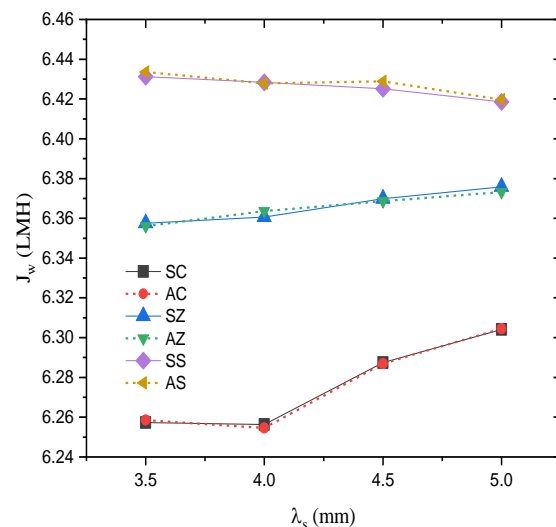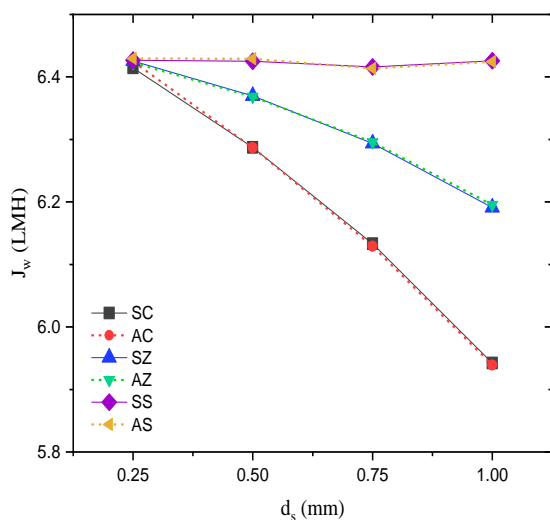


(a) Water flux vs. spacers' diameter at $K = 0.5 \, s.\mu m^{-1}$ ($\lambda_s = 4.5 \, mm$)

(b) Water flux vs. spacers' relative distance at $K = 0.5 \, s.\mu m^{-1}$ ($d_s = 0.5 \, mm$)

**Fig. 7.** Effect of spacers' arrangement on water flux
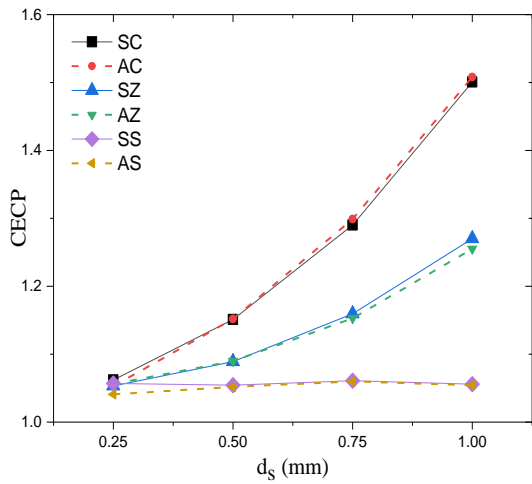
(a) CECP vs. spacers' diameter at $K = 0.5\ s.\mu m^{-1}$ ($\lambda_s = 4.5\ mm$)
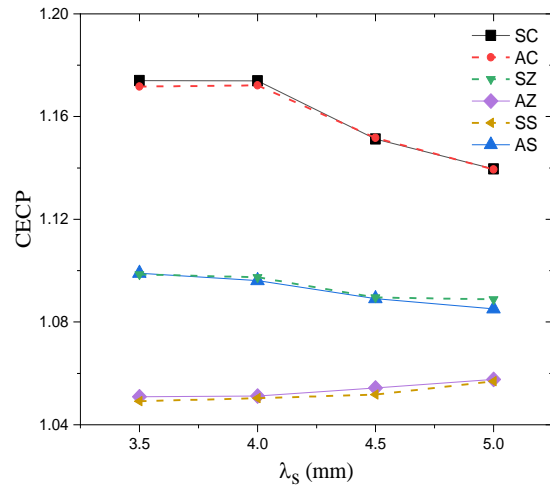
(b) CECP vs. spacers' relative distance at $K = 0.5\ s.\mu m^{-1}$ ($d_s = 0.5\ mm$)
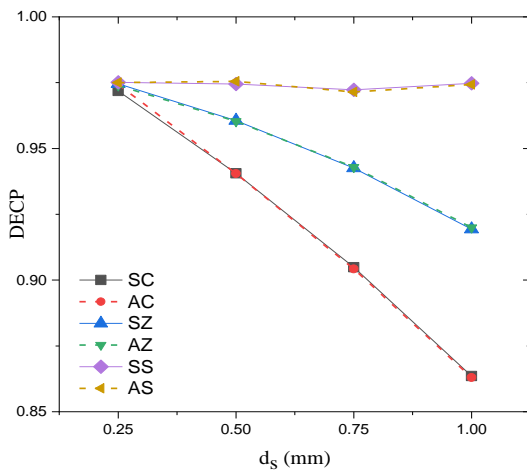
(c) DECP vs. spacers' diameter at $K = 0.5\ s.\mu m^{-1}$ ($\lambda_s = 4.5\ mm$)
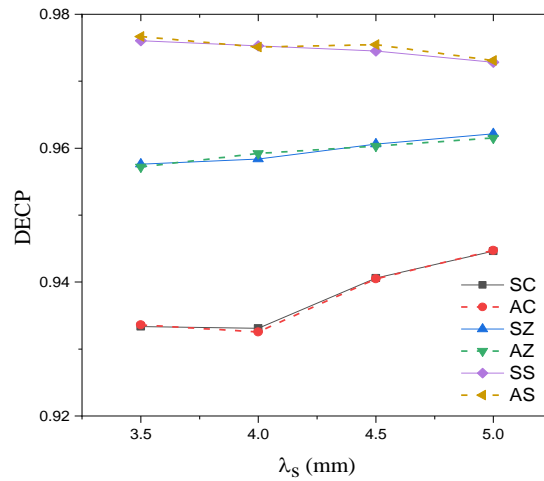
(d) DECP vs. spacers' relative distance at $K = 0.5\ s.\mu m^{-1}$ ($d_s = 0.5\ mm$)

**Fig. 8.** Effect of spacers' arrangement on external concentration polarization factors
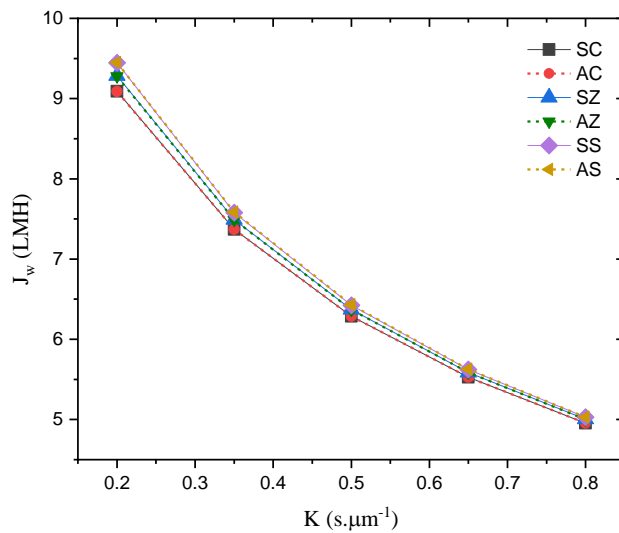


**Fig. 9.** Effect of the solute resistivity of the porous support layer on water flux in different configurations ($d_s = 0.5\ mm$ and $\lambda_s = 4.5\ mm$)

The subsequent tangible influence of the tangent spacers on the membrane surface is membrane fouling, rather than water flux decline. Water flux is basically controlled by the intensity of ICP and the concentration difference between the draw and feed solutions. The value of water flux decreases with the increase of $K$ as higher solute resistivity augments the value of ICP in the membrane porous support layer and declines the effective concentration difference across the membrane active layer. The amount of water flux decline is less severe in the high values of $K$.

In Fig. 10, the values of CECP and DECP have also been computed at different values of $K$ for all the configurations with $d_s = 0.5\ mm$ and $\lambda_s = 4.5\ mm$. As $K$ increases, the value of the ICP in the porous support layer increases, which yields lower effective concentration difference across the membrane active layer. The decrease in the effective concentration difference causes a reduction in the reverse solute flux, $J_s$, which subsequently causes fewer amounts of solute to get trapped in the dead zone. In addition, the decrease in the effective concentration difference leads to the decline of the water flux, $J_w$, which in turn causes less dilution of the draw solution in the dead zone of the draw channel. In the submerged configurations where there is no dead zone, the latter explanation about the less concentration of the feed solution and dilution of the draw

solution on the membrane sides is valid, similarly. The difference between the CECP and DECP values among the different configurations at the same $K$ value is attributed to the difference in the amount of the dead zone, which was discussed earlier.

Finally, we investigate the effect of spacers' arrangement on the feed channel pressure drop per unit length of the membrane. Figure 11 depicts this parameter for different configurations at $K = 0.5\ s.\mu m^{-1}$. Initially, the relative distance changes for $d_s = 0.5\ mm$. As the distance between the spacers decreases, at a fixed spacer diameter, the pressure drop per unit length of the membrane increases. The reason is that the fluid flow faces more obstacles (spacers) in a certain length of the membrane. Also, the effect of different spacers' diameters is studied for $\lambda_s = 4.5\ mm$. As the diameter of the spacer decreases at a fixed spacer distance, the pressure drop per unit length of the membrane increases, which can be explained by the fact that when the diameter of the spacer decreases, the width of the channels decreases accordingly (twice as large as the diameter). Therefore, at a smaller width of the channel, the velocity gradients on the channel wall and membrane surface increase, leading to an increase in the shear force exerted on the channel wall and membrane surface. Hence, the pressure drop per unit length of the membrane increases.
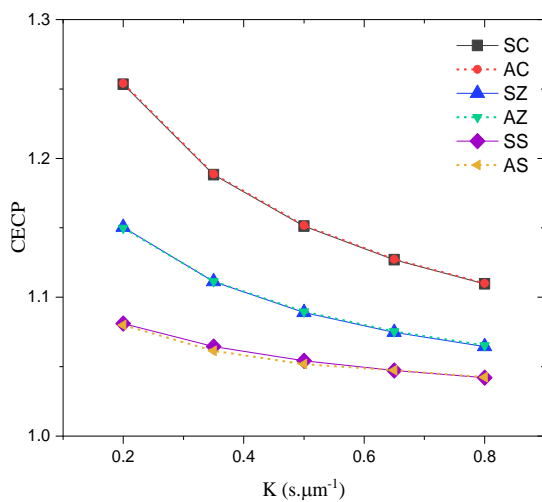


(a)  CECP vs. solute resistivity    (b)  DECP vs. solute resistivity
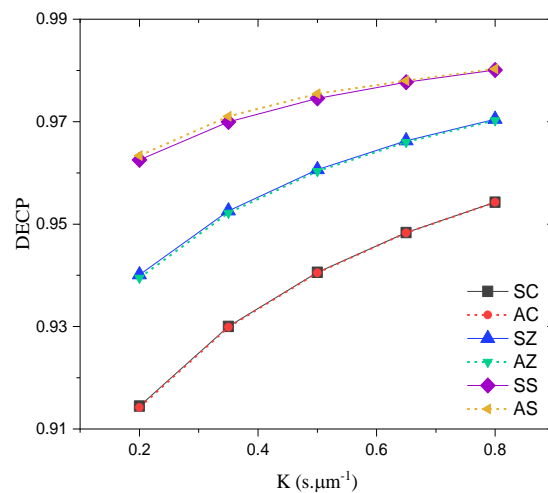
**Fig.10.** Effect of the solute resistivity of the porous support layer on external concentration polarization factors in different configurations ($d_s = 0.5\ mm$ and $\lambda_s = 4.5\ mm$)

The submerged configurations have a considerably higher pressure drop compared with the other configurations. In the submerged configurations, spacers are positioned in the middle of the channels and produce similar and symmetric eddies that augment the shear force on the membrane and wall surfaces. In submerged configurations, each spacer contributes to the increase in the exerted shear force on the membrane surface and channels wall, and the amount of the increase in the shear force on the membrane surface and the channel wall is higher than those of the other configurations. Despite having the minimum ECP and maximum water flux, the submerged configurations show a significantly higher pressure drop per unit length of the membrane. Since the input energy for FO membrane modules is low, the increased pressure drop per unit length of the membrane does not impose a considerably higher cost. However, the use of these spacers while maintaining adequate mechanical support for membrane sheets, and keeping them apart, is impractical. Thus, providing longitudinal filaments in the membrane modules with submerged spacers is necessary.

## 4. Conclusions

In this paper, we presented a two-dimensional numerical study of the FO membranes with feed and draw channel spacers. The steady-state equations corresponding to the conservation of mass, momentum, and transport of solute mass fraction were solved using ANSYS Fluent solver. The appropriate boundary conditions for each equation, and also the geometry of the problem were described.

In this work, we evaluated the performance of FO membrane modules in terms of the spacers' geometrical parameters such as diameter and relative distance, as well as the solute resistivity of the porous support layer for different configurations. Six different types of spacer configurations were considered, which are obtained by the symmetric and asymmetric placement of cavity, submerged, and zigzag configurations. The definition of each type and how the corresponding geometry is created were discussed thoroughly. The performance of the membranes was assessed by the water flux, external concentration polarization factors (CECP, and DECP), and pressure drop per unit length of the membrane in the feed channel.

The correctness of the CFD simulations was verified by comparison with a previously published CFD work in the literature. Also, grid convergence indexes were calculated for the output parameters to find the appropriate mesh size required to resolve the flow features.

Our results showed that increasing the solute resistivity of the porous support layer decreases the water flux. Increasing the spacers' diameter reduces the water flux, although the relative distance between the spacers has a negligible effect. Also, as the solute resistivity increase, CECP decreases,
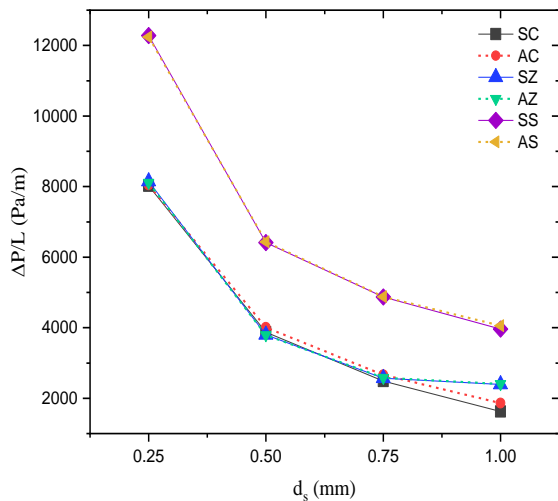


(a) Pressure drop per unit length vs. spacers' diameter at $K = 0.5\ s.\mu m^{-1}$ ($\lambda_s = 4.5\ mm$)
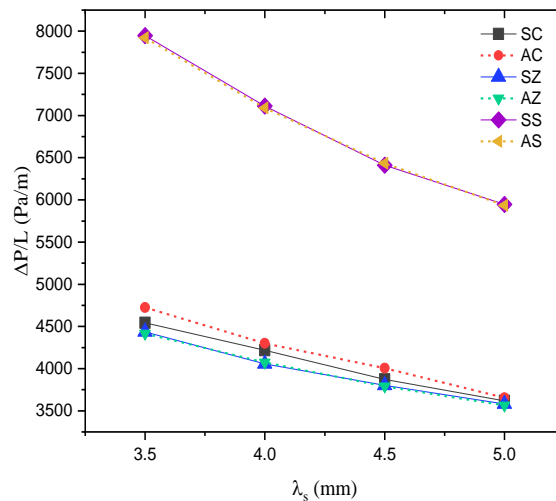
(b) Pressure drop per unit length vs. spacers' relative distance at $K = 0.5\ s.\mu m^{-1}$ ($d_s = 0.5\ mm$)

**Fig.11.** Effect of spacers' arrangement on pressure drop per unit length of the feed channel

and DECP increases. The same pattern is observed when the distance between the spacers increases. However, CECP increases, and DECP decreases with spacers' diameter increase.

Among the spacers' configurations, the submerged arrangements provide the highest water flux and DECP, while producing the least amount of CECP. The trends continue with the zigzag and cavity arrangements afterwards. The cavity configurations showed the highest CECP, and the least DECP factors, due to their highest volume of the dead zone per unit length of the membrane. Although the volume of the dead zone per unit length of the membrane was found to be the major parameter affecting the ECP factors, the amount of ICP was shown to be the limiting factor in water flux decline. It was shown that the variation of the water flux among the different configurations, having different dead zone volumes, was negligible compared to that with the solute resistivity of the porous support layer. Finally, it was observed that the submerged configurations produce the highest pressure drop per unit length of the membrane as they impose more shear force on the membrane surface and the channel wall.

## References

[1] W. Chan, E. Marand, S.M. Martin, Novel zwitterion functionalized carbon nanotube nanocomposite membranes for improved RO performance and surface anti-biofouling resistance, J. Memb. Sci. 509 (2016) 125–137.

[2] J. Farahbakhsh, M. Delnavaz, V. Vatanpour, Investigation of raw and oxidized multiwalled carbon nanotubes in fabrication of reverse osmosis polyamide membranes for improvement in desalination and antifouling properties, Desalination. 410 (2017) 1–9.

[3] R. Ghidossi, D. Veyret, P. Moulin, Computational fluid dynamics applied to membranes: State of the art and opportunities, Chem. Eng. Process. Process Intensif. 45 (2006) 437–454.

[4] A.L. Ahmad, K.K. Lau, M.Z.A. Bakar, Impact of different spacer filament geometries on concentration polarization control in narrow membrane channel, J. Memb. Sci. 262 (2005) 138–152.

[5] A. Hilgenstock, R. Ernst, Analysis of installation effects by means of computational fluid dynamics—CFD vs experiments?, Flow Meas. Instrum. 7 (1996) 161–171.

[6] M. Park, J.J. Lee, S. Lee, J.H. Kim, Determination of a constant membrane structure parameter in forward osmosis processes, J. Memb. Sci. 375 (2011) 241–248.

[7] A. Sagiv, R. Semiat, Finite element analysis of forward osmosis process using NaCl solutions, J. Memb. Sci. 379 (2011) 86–96.

[8] M.F. Gruber, C.J. Johnson, C.Y. Tang, M.H. Jensen, L. Yde, C. Hélix-Nielsen, Computational fluid dynamics simulations of flow and concentration polarization in forward osmosis membrane systems, J. Memb. Sci. 379 (2011) 488–495.

[9] M. Park, J.H. Kim, Numerical analysis of spacer impacts on forward osmosis membrane process using concentration polarization index, J. Memb. Sci. 427 (2013) 10–20.

[10] A. Sagiv, A. Zhu, P.D. Christofides, Y. Cohen, R. Semiat, Analysis of forward osmosis desalination via two-dimensional FEM model, J. Memb. Sci. 464 (2014) 161–172.

[11] M.F. Gruber, U. Aslak, C. Hélix-Nielsen, Open-source CFD model for optimization of forward osmosis and reverse osmosis membrane modules, Sep. Purif. Technol. 158 (2016) 183–192.

[12] M. Kahrizi, J. Lin, G. Ji, L. Kong, C. Song, L.F. Dumée, S. Sahebi, S. Zhao, Relating forward water and reverse salt fluxes to membrane porosity and tortuosity in forward osmosis: CFD modelling, Sep. Purif. Technol. 241 (2020) 116727.

[13] J. Schwinge, D.E. Wiley, D.F. Fletcher, Simulation of the flow around spacer filaments between narrow channel walls. 1. Hydrodynamics, Ind. Eng. Chem. Res. 41 (2002) 2977–2987.

[14] J. Schwinge, D.E. Wiley, A.G. Fane, Novel spacer design improves observed flux, J. Memb. Sci. 229 (2004) 53–61.

[15] O. Kavianipour, G.D. Ingram, H.B. Vuthaluru, Investigation into the effectiveness of feed spacer configurations for reverse osmosis membrane modules using Computational Fluid Dynamics, J. Memb. Sci. 526 (2017) 156–171.

[16]    V. Geraldes, V. Semião, M.N. de Pinho, Flow and mass transfer modelling of nanofiltration, J. Memb. Sci. 191 (2001) 109–128.

[17]    S. Loeb, L. Titelman, E. Korngold, J. Freiman, Effect of porous support fabric on osmosis through a Loeb-Sourirajan type asymmetric membrane, J. Memb. Sci. 129 (1997) 243–249.

[18]    W.H. Press, S.A. Teukolsky, W.T. Vetterling, B.P. Flannery, Numerical recipes 3rd edition: The art of scientific computing, Cambridge university press, 2007.